Zhou, R., Han, Y., Cao, J., Li, M., Jin, G., Du, Y., Luo, H., Yang, Y., Zhang, L., & Su, B. (2018). Enhanced Osseointegration of Hierarchically Structured Ti Implant with Electrically Bioactive SnO_2-TiO_2 Bilayered Surface. *ACS Applied Materials and Interfaces*, *10*(36), 30191-30200. https://doi.org/10.1021/acsami.8b10928

ACS APPLIED MATERIALS & INTERFACES

Biological and Medical Applications of Materials and Interfaces

Enhanced osseointegration of hierarchically structured Ti implant with electrically bioactive SnO2-TiO2 bi-layered surface

Rui Zhou, Yong Han, Jianyun Cao, Ming Li, Guorui Jin, Yuzhou Du, Haoteng Luo, Yongchao Yang, Lizhai Zhang, and Bo Su

ACS Appl. Mater. Interfaces, **Just Accepted Manuscript** • DOI: 10.1021/acsami.8b10928 • Publication Date (Web): 21 Aug 2018

Just Accepted

ACS Publications

is published by the American Chemical Society. 1155 Sixteenth Street N.W., Washington, DC 20036

Enhanced osseointegration of hierarchically structured Ti implant with electrically bioactive SnO_2-TiO_2 bi-layered surface

Rui Zhou [†‡], *Yong Han* [*†], *Jianyun Cao* [⊥], *Ming Li* [⊤], *Guorui Jin* [¶], *Yuzhou Du* [§], *Haoteng Luo* [†], *Yongchao Yang* [†], *Lizhai Zhang* [†], *Bo Su* [*‡]

[†] State Key Laboratory for Mechanical Behavior of Materials, Xi'an Jiaotong University, Xi'an 710049, P.R. China

[‡] Bristol Dental School, University of Bristol, Bristol BS1 2LY, UK

[⊥] School of Materials, University of Manchester, Manchester M13 9PL, UK

[⊤] Honghui Hospital, Xi'an Jiaotong University College of Medicine, Xi'an 710054, P.R. China

[¶] Bioinspired Engineering and Biomechanics Center, Xi'an Jiaotong University, Xi'an 710049, P.R. China

[§] School of Materials Science and Engineering, Xi'an University of Technology, Xi'an 710048, P.R. China

KEYWORDS: Hierarchical structure, Electrical bioactivity, SnO_2-TiO_2, Ti implant, osseointegration.

ABSTRACT: The poor osseointegration of Ti implant significantly compromise its application in load-bearing bone repair and replacement. Electrically bioactive coating inspirited from heterojunction on Ti implant can benefit osseointegration but cannot avoid the stress shielding effect between bone and implant. To resolve this conflict, hierarchically structured Ti implant

with electrically bioactive SnO_2-TiO_2 bi-layered surface has been developed to enhance osseointegration. Benefiting from the electric cue offered by the built-in electrical field of SnO_2-TiO_2 heterojunction and the topographic cue provided by the hierarchical surface structure to bone regeneration, the osteoblastic function of basic multicellular units (BMUs) around the implant is significantly improved. Because the individual TiO_2 or SnO_2 coating with uniform surface exhibits no electrical bioactivity, the effects of electric and topographic cues to osseointegration have been decoupled via the analysis of *in vivo* performance for the placed Ti implant with different surfaces. The developed Ti implant shows significantly improved osseointegration with excellent bone-implant contact, improved mineralization of extracellular matrix (ECM), and increased push-out force. These results suggest that the synergistic strategy of combing electrical bioactivity with hierarchical surface structure provides a new platform for developing advanced endosseous implants.

INTRODUCTION

Ti metal has gained worldwide recognition as one of the most acceptable candidates for load-bearing bone repair materials. [1] However, the osseointegration of Ti implants is often compromised due to the stress shielding effect and its bio-inertness. [2,3] In particular, the lack of mechanical stimulation to bone caused by the stress shielding effect and the poor bone-implant bonding due to the generation of soft tissue on bio-inert pure Ti surface would directly lead to the osteoporosis around the implantation site. Consequently, it eventually results in the failure of the implant. [4-6] As a living tissue, bone can remodel itself around the implantation site to adapt to the

new mechanical environment based on the structure of placed implant. [7] This process is accomplished by assembly of osteoblasts and osteoclasts into functional units, named as basic multicellular units (BMUs). [8] Because the implant surface directly touches with the surrounding environment after surgery, the behavior of cells in the BMUs could be mediated by the surface of implant. Thus, great efforts have been devoted to modifying the structure and surface of Ti implant for improving osseointegration. [9]

Depending on the mechanical properties of composite material, the gradient stress distribution corresponding to hierarchically porous surface of implant with bone tissue could alleviate the stress shielding effect. To obtain the interlocking effect between the implant and bone tissue, the size of gouges on the implant surface should be larger than 50 μm, which can provide enough space for bone ingrowth based on the osseoconduction. [10] The fabrication of hierarchically porous surface with excellent bonding to Ti implant is key to ensure the success of the implant in load-bearing bone repair. Fortunately, the porous surface of TiO_2 coating formed by microarc oxidation (MAO) can be regulated by controlling applied parameter, and the as-formed coating exhibits excellent bonding with Ti substrate. [11-13] Therefore, a multi-scale porous TiO_2 surface with micro gouges and sub-micro pores has been developed on Ti implant via MAO, which enhances mechanical stimulation for improving osseointegration based on the topographic cue from hierarchically structured surface to transmit load. Though the Ti implant with certain hierarchical surface structure exhibits an enhancement in push-out force, soft tissue is still partially covered the implant due to the poor bioactivity of the surface. [14]

In order to achieve a good osseointegration after implantation, numerous strategies have

been developed to facilitate Ti surface with good bioactivity. [15-20] Though chemical and topographical-based coatings are the most promising approaches to render Ti surface with excellent *in vivo* performance, [17-19] their effects to bone tissue around the implantation site are still limited if they have indirect contact with implant surface. Considering the stress shielding effect, osteoporosis would easily occur in certain areas. It is known that bone is a piezoelectric material, in which electric cue offered by externally applied electrical fields can modulate osteoblastic cell behavior. [21,22] Since the bone tissue can conduct electrical signal, the electric cue could not only affect the contact interface but also influence the indirectly-contacted surrounding area of the implant. However, electric cue provided by an external equipment is impractical for orthopedic implant application. [23] To realize such a concept, developing Ti implant with an internally built-in electrical field would be critical for the next-generation of implant. [23-25]

A promising strategy for the fabrication of such an internally built-in electrical field is based on the concept of heterojunction, which promotes the separation of hole-electron pairs. [25-27] Meanwhile, because of the electric coupling among different electrical fields, [28] the heterojunction with the built-in electrical field can continuously provide electric cue to ensure a long-term effect of the electrical bioactivity based on the response to varied electrical field from piezoelectric bone during movement. [29] Interestingly, a built-in electrical field on smooth Ti plate via the formation of bi-layered SnO_2-TiO_2 heterojunction with type II band alignment was reported in our previous work, which exhibited superhydrophilicity and good apatite-forming ability. [30] To render the hierarchically porous Ti implant with excellent bioactivity, in this work, the bi-layered SnO_2-TiO_2 heterojunction was fabricated on the surface of hierarchically

structured Ti implant by MAO and subsequent hydrothermal treatment.

Because the individual TiO_2 or SnO_2 coating with an uniform surface does not exhibit bioactivity induced by electric cue, it provides a platform to decouple the effects of electric cue and topographic cue to osseointegration via the comparison of the bone remodeling, bone-implant interface, and biomechanical property for the prepared Ti implants with different surface structures.

RESULTS AND DISCUSSION

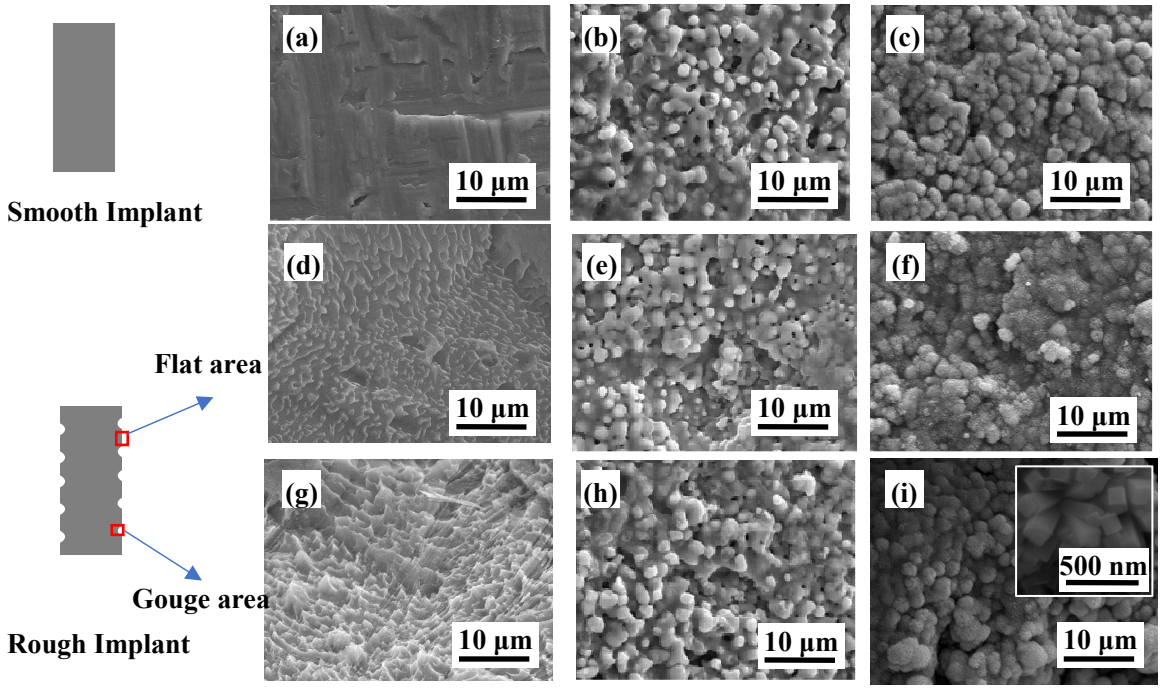

Figure 1 Surface morphologies of modified Ti implants with different structures: a) Ti, b) Ti-TiO_2, c) Ti-TiO_2-SnO_2; flat area of d) R-Ti, e) R-Ti-TiO_2, f) R-Ti-TiO_2-SnO_2; and gouge area of g) R-Ti, h) R-Ti-TiO_2, i) R-Ti-TiO_2-SnO_2.

To ensure a uniform structure of the developed coating at the different areas (flat area and

gouges area) of the implant, the Ti implant surface with micro gouges has been acidly etched to remove the non-uniform oxide film before subsequent treatments. The reason for the acid etching is that the non-uniform oxide film would lead to changes in morphology and phase composition of the as-formed MAO coating in the different areas according to our previous investigation. [31] As shown in Figure 1, the surface with a morphology of acidly etched pits has been formed on the surface of rough Ti implant in both flat and gouge area. According to the EDS results, there is no oxide film left on the implant surface (Figure S1). Therefore, the reaction during the subsequent MAO treatment to the implant could occur homogeneously in both flat and gouge areas, retaining to uniform surface morphology on the whole surface. A sub-micro porous layer after MAO treatment (Figure 1(b,e,h)) and a layer of nanorod array after hydrothermal treatment (Figure 1(i) and S2) are observed. In the following, the implants are labeled according to their structure as shown in Table S1, which is divided into two groups, smooth group (Ti, Ti-TiO_2, Ti-TiO_2-SnO_2) and rough group (R-Ti, R-Ti-TiO_2, R-Ti-TiO_2-SnO_2), based on the different surface structures. Owing to the generation of gouges on the rough implant, a mass loss of the implants has been measured, showing the porosity of the rough implants is 18.2 ± 0.2% (Figure S3).

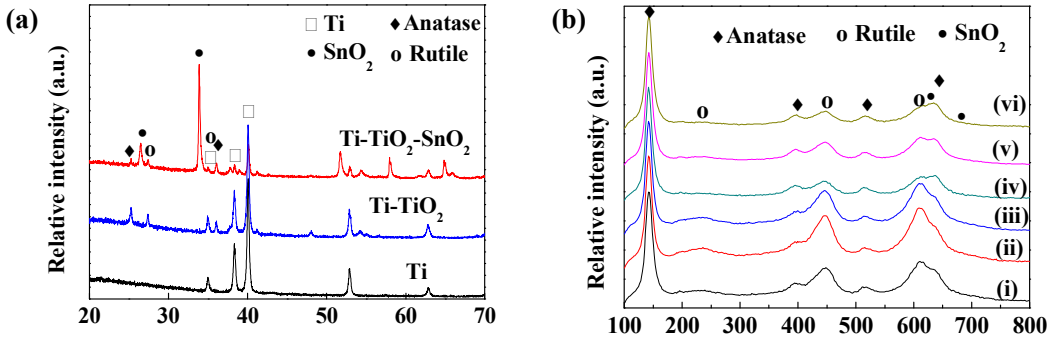

Figure 2 a) XRD patterns of Ti, Ti-TiO_2 and Ti-TiO_2-SnO_2; b) Raman spectra of coated implants detected from different area: i) Ti-TiO_2, ii) flat area of R-Ti-TiO_2, iii) gouge area of R-Ti-TiO_2, iv) Ti-TiO_2-SnO_2, v) flat area of R-Ti-TiO_2-SnO_2, and vi) gouge area of R-Ti-TiO_2-SnO_2.

Regarding the heterojunction, the crystallinity of designed phase is the key to its performance. [32-34] The amorphous MAO coating with SnO_2 film cannot form a heterojunction with electrically stimulated bioactivity because it cannot obtain a stable Fermi energy of TiO_2 to promote the separation of hole-electron pairs. [30] To meet the formation requirement of heterojunction with type II aligned structure, [35,36] a high voltage had to be applied to fabricate the MAO coating with good crystallinity. As expected, TiO_2 based MAO coating and the SnO_2 film were formed on Ti substrate after the subsequent treatments as indicated in the XRD patterns (Figure 2(a)).

To further confirm the phase composition of the coating generated on the implant with micro gouges, Raman spectroscopy has been employed to characterize the coating in both gouges area and flat area. Consistent with the XRD results, similar Raman spectra of the MAO coating with two different phases of TiO_2 have been detected from different areas of Ti-TiO_2 and R-Ti-TiO_2,

revealing that the gouge does not affect the phase composition of MAO coating (Figure 2(b)). The Raman modes centered at 144, 399, 519 and 639 cm^{-1} are pointed to the anatase phase TiO_2, [37] while the Raman modes centered at 240, 446 and 609 cm^{-1} are assigned to the rutile phase TiO_2. [38] As for the nanorods film, Raman spectra detected from both the gouge and flat areas show similar characteristic vibration modes of SnO_2, which are centered at 629 and 689 cm^{-1}, [39] respectively (see in Figure S4). Both the XRD and Raman results indicate a uniform SnO_2-TiO_2 bi-layer was fabricated on the surface of Ti-TiO_2-SnO_2 and R-Ti-TiO_2-SnO_2, which is in good agreement with the bi-layered SnO_2-TiO_2 coating on Ti plate reported in our previous work. [30]

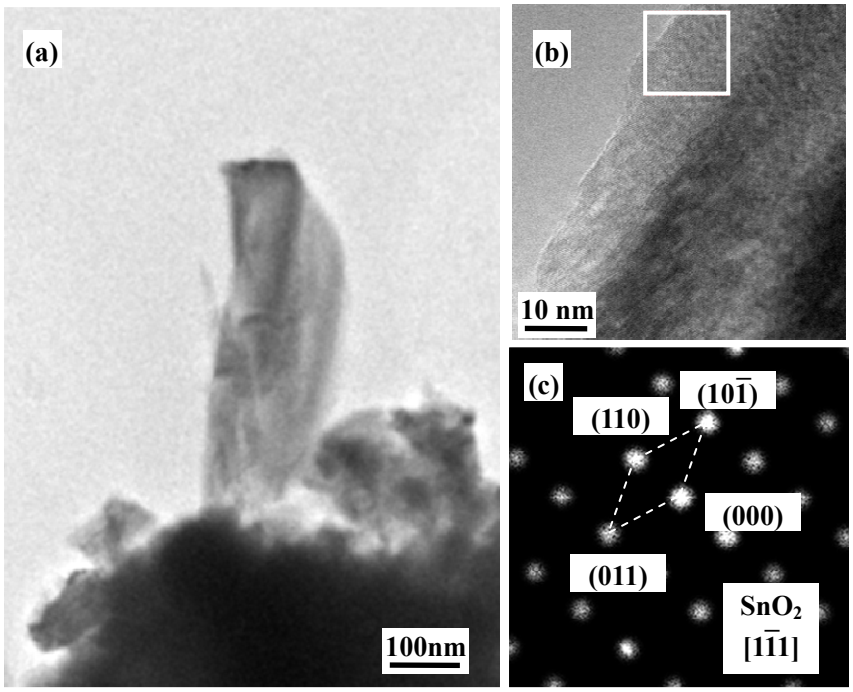

Figure 3 a) the TEM morphology of the powder collected from R-Ti-TiO_2-SnO_2, b) high resolution TEM morphology of nanorod and c) selected area electron diffraction pattern obtained by Fast Fourier Transform technique from the white box area.

To further confirm the structure of SnO_2-TiO_2 coating formed on the R-Ti-TiO_2-SnO_2, TEM

has been used to analyze the powder collected from its surface (Figure 3). Clearly, the nanorod is mainly composed of Sn and O as confirmed by the EDS results. The selected area electron diffraction (SAED) pattern of the nanorod obtained by the Fast Fourier Transform (FFT) technique further confirms its phase of SnO_2 (Figure 3 (c)). Thus, we can confirm that SnO_2 nanorods film was generated on the R-Ti-TiO_2-SnO_2 surface.

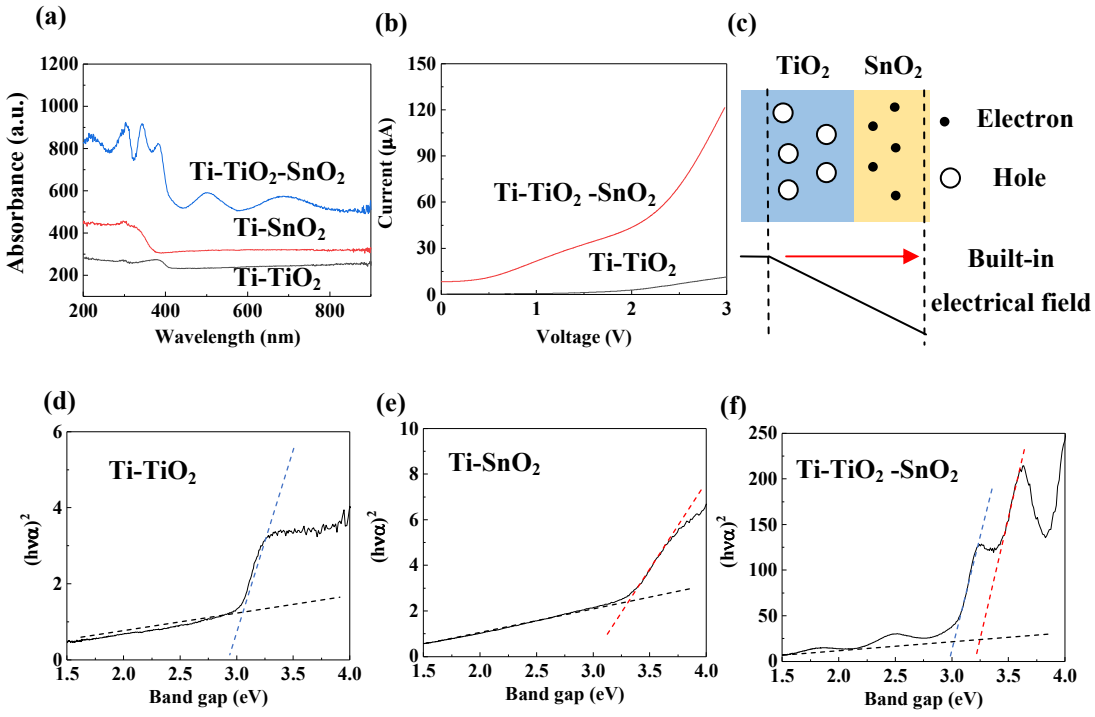

Figure 4 a) UV-vis absorption spectra of Ti-TiO_2, Ti-SnO_2, and Ti-TiO_2-SnO_2, b) LSV curves of Ti-TiO_2, and Ti-TiO_2-SnO_2, c) schematic diagram for the built-in electrical field of SnO_2-TiO_2 heterojunction, and the plots of $(\alpha hv)^2$ versus hv of d) Ti-TiO_2, e) Ti-SnO_2, f) Ti-TiO_2-SnO_2.

Due to the similar phase composition and structure of the bi-layered SnO_2-TiO_2 coating with our previous work on Ti plate, [30] an n-n heterojunction could be formed on the R-Ti-TiO_2-SnO_2 surface. To confirm the formation of the SnO_2-TiO_2 heterojunction, the band gap of the

bi-layered SnO_2-TiO_2 coating has been determined by UV-vis spectrophotometer using Ultra Violet Diffuse Reflectance Spectroscopy technique (Figure 4). Based on the UV absorption spectral data, the direct band gaps can be obtained by Tauc relation with a linear fit via the equation: [40] $(\alpha hv)^2 = A \cdot (hv - E_g)$, where α is absorption coefficient, A is the proportionality constant, hv is the photon energy, and E_g is the energy band gap. Clearly, individual TiO_2 or SnO_2 film shows typical semi-conductor feature, with the calculated band gap of 3.01 and 3.38 eV, respectively. As for the Ti-TiO_2-SnO_2, the band gaps of both TiO_2 layer and SnO_2 layer are observed, indicating the formation of SnO_2-TiO_2 heterojunction. Interestingly, two peaks around 700 and 510 nm are also observed in the UV-vis absorption spectrum of Ti-TiO_2-SnO_2 (Figure 4(a)), indicating that electrons on Ti-TiO_2-SnO_2 surface can transfer to conduction band (CB) with lower excited energy than that of individual TiO_2 or SnO_2. This result further confirms the formation of SnO_2-TiO_2 heterojunction, because the separated electrons and holes with the metastable status have already been stimulated by the built-in electrical field of heterojunction, resulting in the reduced energy for photoelectronic excitation to overcome the energy barrier. In addition, according to Figure 4(b), the Linear sweep voltammetry (LSV) curve of the Ti-TiO_2-SnO_2 coating shows significantly larger response current than that of the Ti-TiO_2, suggesting better electrical conductivity of the coating due to the formation of heterojunction thus higher charge carrier density. Such SnO_2-TiO_2 coating exhibits superhydrophilicity, good apatite-forming ability, and negative surface potential, leading to good electrical bioactivity. [30] Combined with the hierarchical structure of Ti implant, the synergistic effect of hierarchical surface structure and electrical bioactivity for the developed Ti implants on osseointegration has

been investigated.

Normally, bone is considered as a dynamic living tissue which is constantly being remodeled throughout its lifetime, it can adapt its mass and architecture to mechanical demands according to the Wolff's law. [41] To evaluate the status of bone remodeling around the placed Ti implants with different surface structure, the biological tissue around the implants in the region of interest (ROI) ($\Phi 3 \times L6$ mm^3) have been analyzed by micro-CT after healing for 12 weeks.

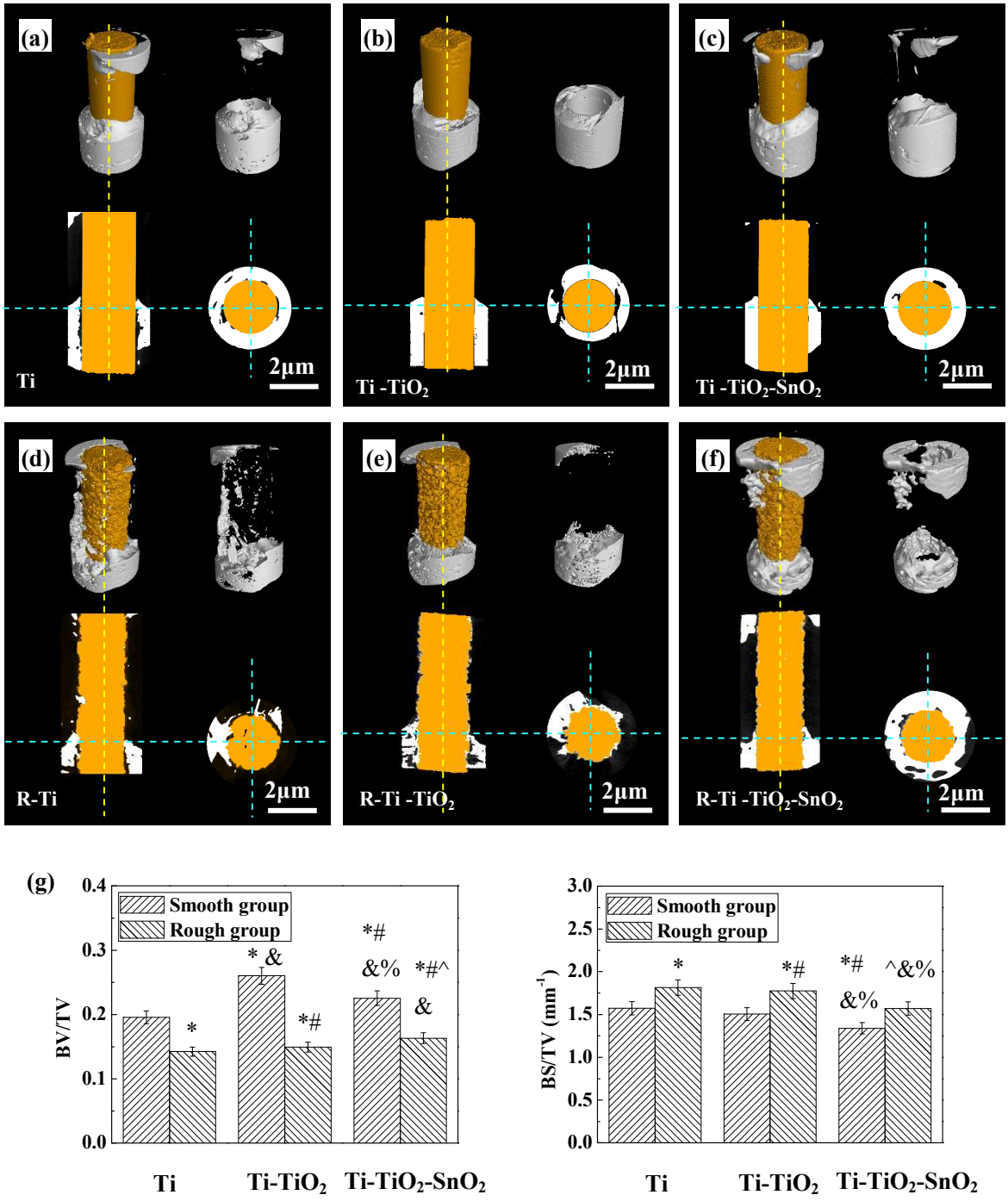

Figure 5 Micro-CT analysis of the biological tissue around implants after surgery for 12 weeks: micro-CT images of a) Ti, b) Ti-TiO_2, c) Ti-TiO_2-SnO_2, d) R-Ti, e) R-Ti-TiO_2, f) R-Ti-TiO_2-SnO_2, and g) the morphometric results in the ROI. *$p < 0.05$ compared to the Ti implant, #$p < 0.05$ compared to the Ti-TiO_2, ^p

< 0.05 compared to the Ti-TiO_2-SnO_2, &p < 0.05 compared to the R-Ti, %p < 0.05 compared to the R-Ti-TiO_2.

According to the cross-sectional morphology of the reconstructed micro-CT images, the biological tissue exhibits a trend to grow along the implant surface towards the marrow cavity (Figure 5). Meanwhile, the biological tissue-implant interface of both the smooth and rough groups shows a similar status with the varied surface structures (the indirect contact for Ti and R-Ti, the partial direct contact for Ti-TiO_2 and R-Ti-TiO_2, and the almost prefect direct contact for Ti-TiO_2-SnO_2 and R-Ti-TiO_2-SnO_2). As for the Ti and R-Ti implants, they are separated from the biologic tissue by gaps due to the bio-inert nature of pure Ti, leading to the indirect contact with bone. Therefore, they both show the least amount of remodeling biological tissue around the implant (Figure 5(a,d)). With regard to the Ti-TiO_2 and R-Ti-TiO_2, the biological tissue partially contacts with the implant surface, while cavities also appear in the bone near certain area (Figure 5(b,e)). The formation of the cavities could be attributed to the stress shielding effect between the implant and bone, which stimulates osteoclasts to resorb more bone in the decreased levels of stress direction. [7] However, owing to the relatively better bioactivity of TiO_2 coating than that of pure Ti, new biological tissue has been generated toward the direction of marrow cavity around the implant to ensure load bearing capability during the bone healing process. Nevertheless, it still shows a relatively loose structure around R-Ti-TiO_2 (Figure 5e). This is strongly supported by the additional statistical analysis for the ROI (Figure 5(g)), where biological tissue with large surface area is obtained, indicating more cavities are detected from the biological tissue around the implant when compared with the R-Ti-TiO_2-SnO_2. In the case of the implants with SnO_2-TiO_2 bi-layered coating, they exhibit the densest structure with excellent biological

tissue-implant contact. The reason for this is attributed to the electrical bioactivity of the coating, which benefits not only the directly contacted tissue, but also the surrounding tissues due to the effect of electrical field.

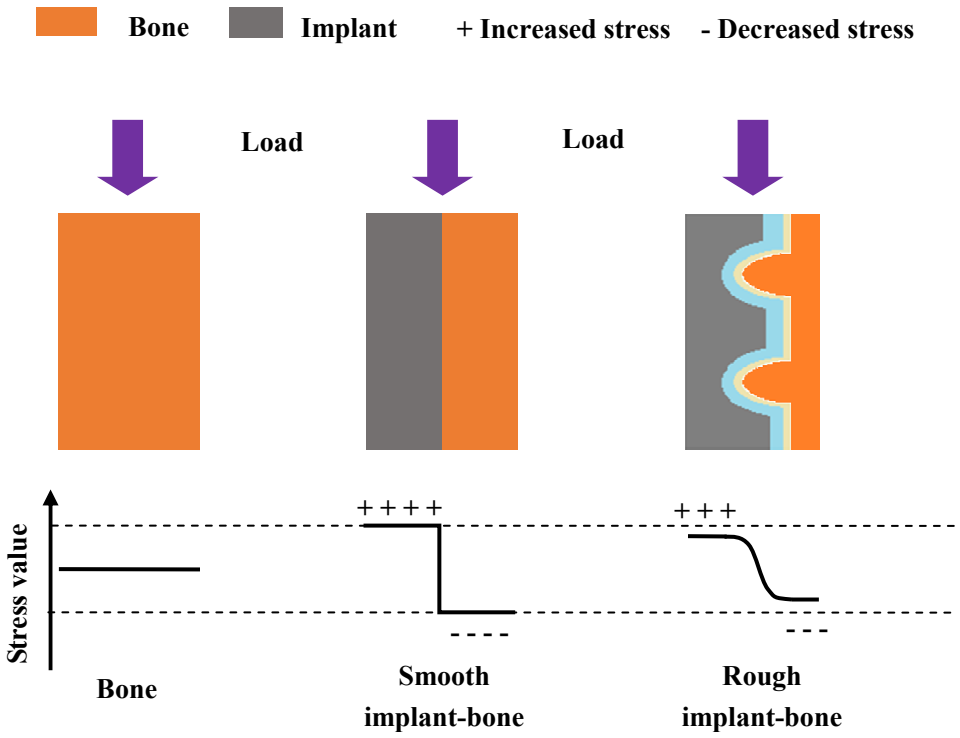

Figure 6 Schematic diagram for the stress distribution at the interface between bone and implants along the radial direction.

Apparently, the structure of biological tissue around the placed implant after healing of 12 weeks depends on the hierarchical structure of the implant surface (Figure 5). This is in agreement with the result that the stress distribution within the bone tissue is related to the recruitment and activity of BMU. [7,42] After the ingrowth of new bone into the micro scale gouges, the placed implant with surrounding bone tissue can be considered as a composite material, which significantly changes the stress distribution in the bonding area (Figure 6). During the

remodeling process in cortical bone, osteoclasts could be observed on the surface of an area with reduced stress, and osteoblasts could be found on the surface of an area with increased stress. [7,42] If a material is with hierarchical bonding interface, the stress on the bone tissue side is decreased but with an increasing trend toward the interface to implant. The decreased stress could promote osteoclast to resorb bone along certain direction, while the increase of stress could stimulate osteoblast to aid remodeling at the interface. [43] Thus, more cavities but better bone-biological contact were observed around the R-Ti and R-Ti-TiO_2 when compared with the smooth group.

Because of the existence of artifacts, soft tissue and mineral bone are hard to be distinguished by the Micro-CT analysis. To further support our point about the BMU coupling, histological morphometry of the Van Gieson (VG) stained bone tissue within 500 μm to the surface of implant has been investigated (Figure 7). Apparently, the cavities containing osteoclast and osteoblast can be clearly observed in the magnified histological morphology around implants. As the functional unit for bone remodeling, BMUs is considered as the most obvious agent to adjust and reveal the bone healing situation around the implant surface in micro scale. [44-48] Disturbances of any stimulation that shift the equilibrium of BMUs would lead to the change in bone remodeling around implants. [49] Herein, the change in size of cavity containing BMU is mainly attributed to two factors of the as-formed implants, the bioactivity of coating and the micro gouge structure.

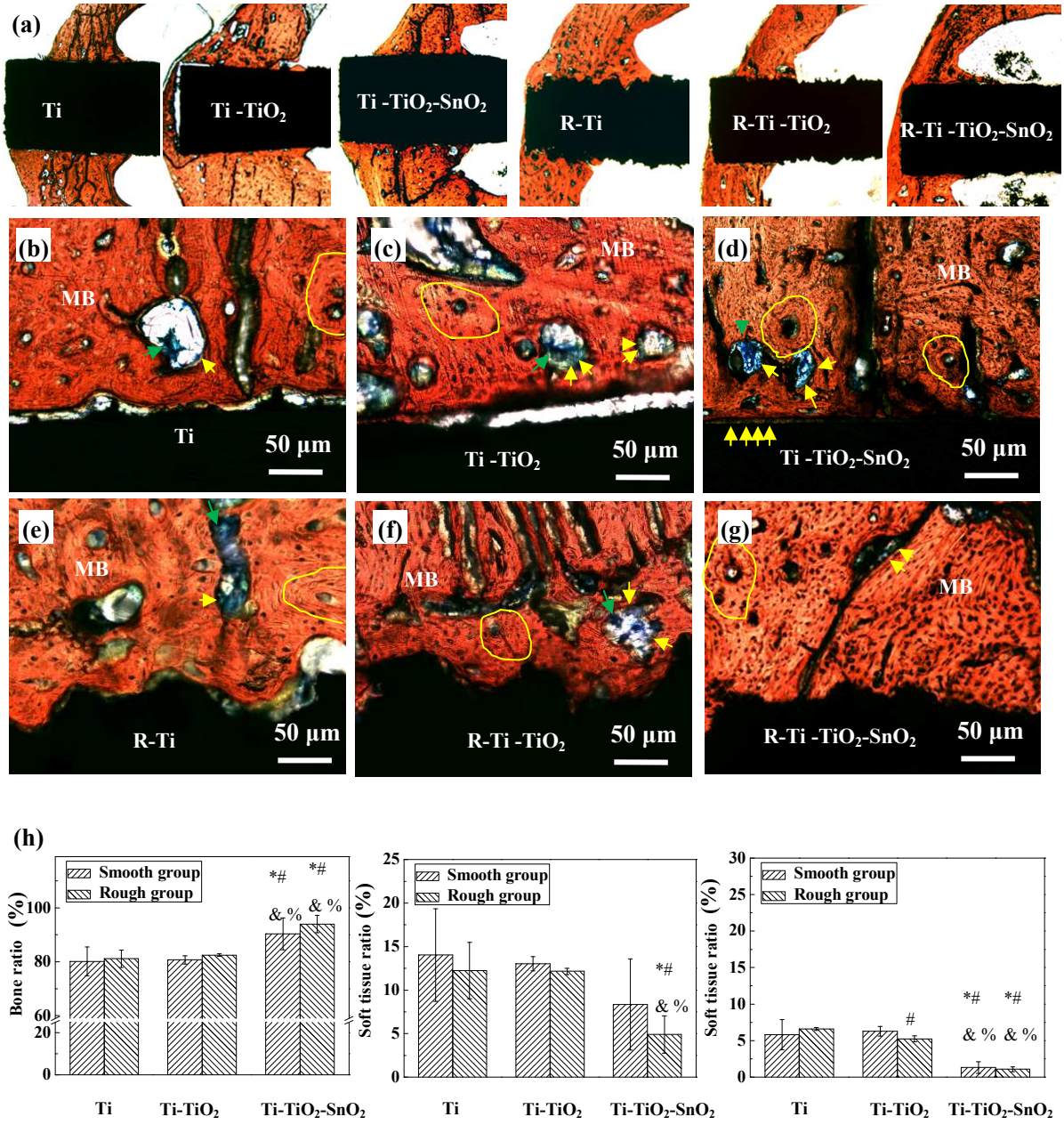

Figure 7 Histological analysis of the bone around the implants after surgery for 12 weeks: a) gross morphologies of the VG stained bone tissue around implants , the representative histological morphology of b) Ti, c) Ti-TiO_2, d) Ti-TiO_2-SnO_2, e) R-Ti, f) R-Ti-TiO_2, g) R-Ti-TiO_2-SnO_2, and h) the histomorphometric results of mineralized bone, soft tissue and gap in the interested zoon. (yellow arrow) osteoblasts; (green arrow) osteoclasts; (yellow ring) osteon; (MB) mineralized bone. *p < 0.05 compared to the Ti implant, #p < 0.05

compared to the Ti-TiO_2, ^p < 0.05 compared to the Ti-TiO_2-SnO_2, &p < 0.05 compared to the R-Ti, %p < 0.05 compared to the R-Ti-TiO_2.

As for the smooth surface group, the behavior of BMUs is dominated by the bioactivity of the implant surface. Generally, the equilibrium of BMUs around implants shifts towards bone resorption after implantation, due to the decrease of stress stimulation to bone tissue caused by the stress shielding effect. Regarding the Ti implant, the surrounding tissue normally shows osteoporosis due to the bio-inertness of pure Ti (Figure 7(b)), which is unable to promote osteoblastic functions (such as proliferation, migration, differentiation, secretion of matrix proteins, and its mineralization) to rebalance the equilibrium of BMUs. [50]

In terms of Ti-TiO_2, the MAO coating with porous surface structure in sub-micro scale can enhance the proliferation and differentiation of osteoblasts. [51] Meanwhile, the TiO_2 coating with negative surface charges can attract Ca^{2+} and proteins absorption. [52] They all shift the equilibrium of BMUs around the implant surface towards the bone generation, playing a positive role in osseointegration. Thus, a direct bone-implant contact has been observed around the implant surface near the marrow cavity (Figure 7(c)). However, because of the relatively weak Ca^{2+} attraction for TiO_2 surface and the indirect contact of the surface with both the cell and proteins from medullary cavity fluid, some surface of the Ti-TiO_2 is still partially separated by gaps or soft tissue near the implantation site. It should be noticed that cavities with osteoclast cell have also been observed in the indirectly contacted bone tissue around Ti-TiO_2 (Figure 7(c)), indicating that the positive effect of the MAO coating on BMUs for bone generation is only limited in the directly contacted area.

Though the Ti-TiO_2-SnO_2 shows similar surface roughness with Ti-TiO_2, the equilibrium of BMUs around it shifts significantly towards the generation of new bone. This phoneme is obviously dominated by the electrical bioactivity of the bi-layered coating rather than the nano-topography of the SnO_2 surface, as the densely packed SnO_2 nanorods would not benefit focal adhesion assembly of cells. [30,53,54] Specifically, transient receptor potential melastatin 7 (TRPM7) protein is one of the signaling pathways on plasma membranes, exhibiting spontaneously activated divalent cation (Ca^{2+}, Mg^{2+}) entry, which is important for osteoblast differentiation. [55,56] Because the surface of SnO_2-TiO_2 heterojunction with negative zeta potential can attract Ca^{2+} and Mg^{2+} absorption, [30] the functional activity of TRPM7 would be ensured under the culture conditions with high intracellular Ca^{2+} or Mg^{2+} concentrations, benefiting the osteoblast differentiation of mesenchymal stem cells around implant. [57,58] Therefore, a cement line interface has been observed on the surface Ti-TiO_2-SnO_2 (Figure 7(d)). Meanwhile, larger amount of osteoblast cells has been proliferated in the cavities around Ti-TiO_2-SnO_2 when compared with the others.

Regarding to the rough implants with micro gouge structure, it is obvious that the osseointegration has improved when compared with the smooth surface with the same modified coating (Figure 7). This is attributed to the changes in the absorption of cells and proteins and the topographic cue for the surrounding tissue based on the implant structure. Firstly, the migration and proliferation of osteoblast or stem cell and absorption of matrix proteins has been accelerated by the gouges surface structure because of its storage ability for the medullar cavity liquid. Secondly, the space provided by surface gouges changes the topographic cue to the surrounding

bone tissue. The micro gouges are very similar to the structure of proceed osteonal tunneling with BMUs, which would be quickly refilled by osteoblast. [7] Thus, the equilibrium of BMUs around the rough implants with micro gouges shifts towards the bone formation.

Associated with the electrical bioactivity of SnO_2-TiO_2 coating and the surface gouge structure, the attraction of Mg^{2+} and Ca^{2+} by the built-in electrical field would be significantly enhanced by the superposition of the electrical field based on the micro gouges structure. Thus, more Mg^{2+} and Ca^{2+} would enrich around the Ti-TiO_2-SnO_2 surface. It could ensure the functional activity of TRPM7, [57,58] showing excellent osseointegration around the implant (Figure 7(g)).

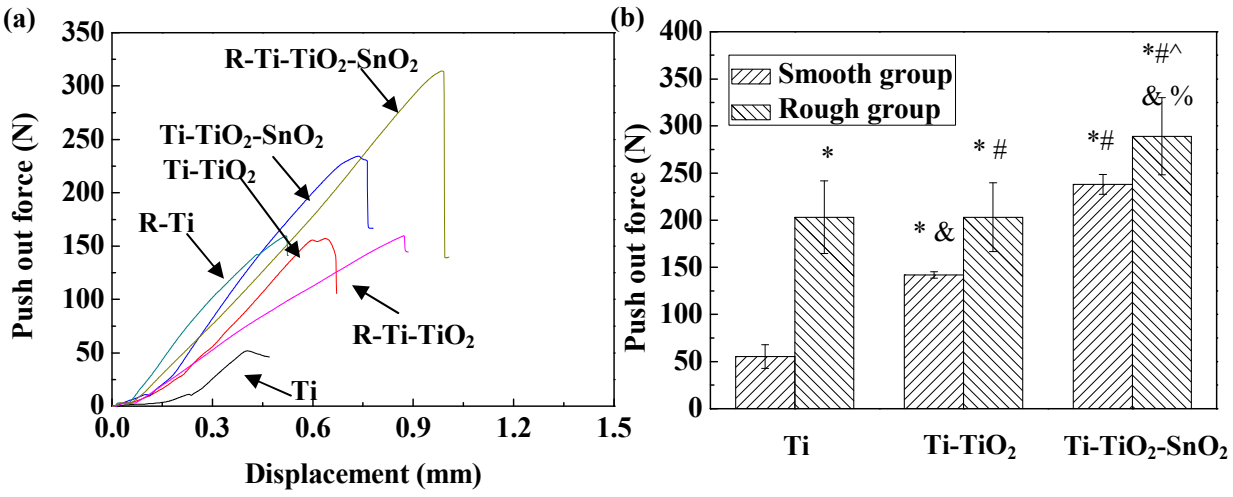

Figure 8 Biomechanical results of the implants after surgery for 12 weeks: a) the typical displacement curves of the implants during the push-out process, b) the push-out force of the implants with different surface structures. *p < 0.05 compared to the Ti implant, #p < 0.05 compared to the Ti-TiO_2, ^p < 0.05 compared to the Ti-TiO_2-SnO_2, &p < 0.05 compared to the R-Ti, %p < 0.05 compared to the R-Ti-TiO_2.

To evaluate the long-term bonding between the developed implant and bone tissue, the

push-out forces for the implants after healing of 12 weeks have been studied (Figure 8). As expected, both the electrically bioactive coating and the gouges structure surface exhibit an increase in the push-out force. In the case of the smooth implant group, the enhancement in the push-out force is dominated by the bioactivity of the implant surface. Obviously, the push-out force of the implant with SnO_2-TiO_2 is significantly improved to 239 N, which is over 5 times that of the pure Ti (50 N) ($p<0.05$). As for the rough implants with micro gouges, though it has less amount of remodeled bone around the implants, they exhibit much higher push-out force than the smooth ones (Figure 8). In consistent with our previous work, [14] no matter how the bone-implant contact is, the push-out force for R-Ti and R-Ti-TiO_2 is similar. The reason for this could be attributed to the meshed bone-implant interface, which changed the failure mode of the implant when compared with the smooth ones. Interestingly, the push-out force of R-Ti-TiO_2-SnO_2 is further increased to 289 N, which is much stronger than that of R-Ti-TiO_2 and R-Ti. This supports our analysis that the electrical bioactivity benefits the osteoblastic function, leading to increased mineralization of extra-cellular matrix (ECM) around the developed implant to transmit load efficiently.

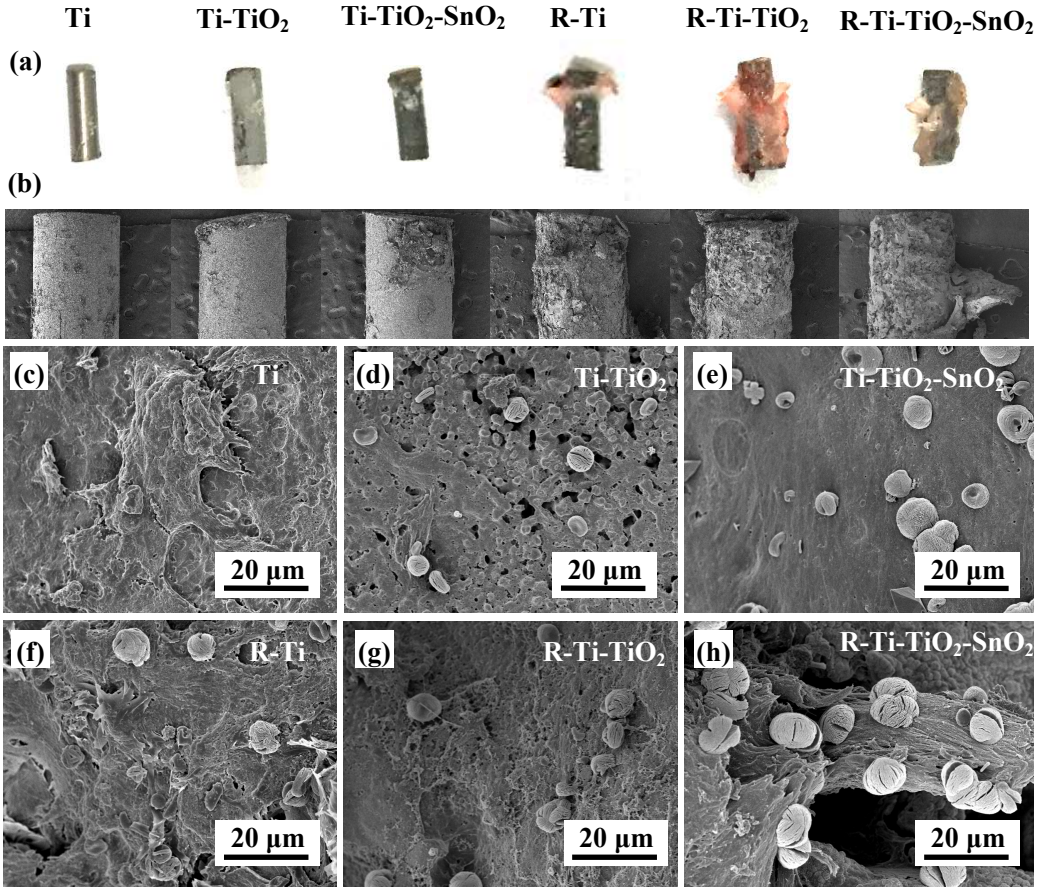

Figure 9 Surface morphologies of the pushed-out implants after healing of 12 weeks: a) gross images of the pushed-out implants, b) SEM images of the pushed-out implant surfaces with biological tissue at the cortical bone area, magnified SEM morphologies of the implant surface c) Ti, d) Ti-TiO_2, e) Ti-TiO_2-SnO_2, f) R-Ti, g) R-Ti-TiO_2, h) R-Ti-TiO_2-SnO_2.

To confirm the failure mode of the implants, representative SEM images of the pushed-out implant in the cortical regions are investigated together with EDS. Clearly, larger amount of biological tissue with meshed structure is observed on the rough implant surfaces compared to the smooth ones (Figure 9). As for the smooth group, pure Ti implant is partially covered by soft tissue, leading to poor contact with surrounding bone tissue, while some deposition with the

shape of distorted sphere in multi-flakes (Ca 14.1 wt. % and P 1.4 wt. %) have been observed on the Ti-TiO_2 surface because of its bioactivity. As expected, a large amount of remnants bone (Ca 78.5 wt. % and P 12.2 wt. %) and sphere-like deposition (Ca 27.2 wt. % and P 6.1 wt. %) have been observed on the surface of Ti-TiO_2-SnO_2. The above evidence directly supports our analysis that the electrically bioactive coating can significantly improve the mineralization of the remodeled bone tissue through the attraction of Mg^{2+} and Ca^{2+}, providing ions signal via the path way of TRM7 on the plasma membrane to accelerate the osteoblastic functions. Further analysis on the fracture morphology in the cortical bone area of the implant shows that some part of the coating on the Ti-TiO_2-SnO_2 has been pulled out with the bone tissue (Ti 78.8 wt. % and C 8.8 wt. %) (Figure S5), indicating the synostosis in the cortical region. As for the rough group, the micro gouges on the R-Ti-TiO_2-SnO_2 surface around the cortical bone side are almost fully filled by dense mineral bone, and fracture mainly occurs at the bone side with large amount of Ca, P and Mg enriched sphere-like depositions (Figure 9). On the contrary, smaller amount of Ca, P and Mg enriched sphere-like depositions has been observed on R-Ti-TiO_2. This result is in agreement with Couchourel's suggestion that the culture conditions with low extracellular Mg^{2+} and Ca^{2+} concentrations promotes gene expression of collagen type I alpha 1, resulting in reduced mineralization of ECM because of the abnormal ratio of matrix protein. [59] This further supports our analysis that the electrical bioactivity provided by SnO_2-TiO_2 hetero-junction would benefit the mineralization of the indirect contact bone tissue around the implant, resulting in a significant improvement in osseointegration of the developed implant.

Recently many strategies have been developed to improve the osseointegration of Ti implant.

Compared with dense Ti implant, the scaffold Ti implant shows obviously enhanced push-out force thanks to the three-dimensional inter-locking effect for the new bone which grows into the holes after healing. [10,60-63] Similar to the scaffold Ti implant, in this work, regenerated bone tissue also meshed with the rough implant in the gouge areas. While, since the fixed porosity of the rough implants limits the ingrowth of bone tissue, the further enhancement in push-out force of R-Ti-TiO_2-SnO_2 is attributed to the increased mineralization of ECM around the implant with synostosis. Comparing the push-out stress with the literature values (seeing in supporting information Table S2), it suggests that the R-Ti-TiO_2-SnO_2 shows the most improved performance, even better than that of surface chemically modified Ti scaffold. Taking the results together, the R-Ti-TiO_2-SnO_2 with the synergistic effects of both electrical bioactivity and hierarchical surface structure has been demonstrated as an efficient approach to enhance osseointegration.

CONCLUSION

Hierarchically porous surface with SnO_2-TiO_2 heterojunction has been fabricated on Ti implant. The significantly improved osseointegration is attributed to electrical bioactivity and hierarchical surface structure of the developed implant. The electrical bioactivity rendered by the bi-layered SnO_2-TiO_2 coating on the implant benefits not only the contacted biological tissue but also the indirectly contacted one thanks to the generation of electrical signal. It improves the osteoblastic function of BMUs, leading to increased mineralization of ECM around the implant with synostosis. Thanks to the topographic cue from the hierarchically porous surface, the newly

formed bone tissue grows into the micro gouges of rough implant, exhibiting meshed bone-implant interface. Meanwhile, the osteoblastic function of BMUs is improved compared to the smooth ones, because the space provided by gouges can act as a storage of medullar cavity liquid, promoting the absorption of matrix proteins and attachment of cells. Benefiting from the superposition of the built-in electrical field provided by heterojunction on the hierarchically porous surface, the mineralization of the remodeled bone around the developed Ti implant is further enhanced, exhibiting excellent *in vivo* performance. Therefore, the concept of hierarchically structured Ti implant with electrically bioactive surface could be a promising approach for developing the next-generation of load-bearing Ti implants, since it benefits from both electric and topographic cues to the living bone.

EXPERIMENTAL SECTION

Surface modification. The medical Ti rods with the size of Φ2 × L6 mm^3 (Grade II, Baoji Haibao special metal materials Co., China) were used as Ti implants for the surface modification and animal surgery. Firstly, the rods were ground with 1000# abrasive paper, ultrasonically washed with acetone, ethanol and distilled water. The micro scale gouges were prepared on Ti implant surface via microarc oxidation (MAO) in an electrolyte containing $NaNO_3$ (0.1 $M \cdot L^{-1}$) and NaOH (0.25 $M \cdot L^{-1}$) at 280 V for 2 min, then acidly washed in 48 wt.% H_2SO_4 at 80 °C for 2 h. To fabricate sub-micro scale porous coating on Ti, the implants were microarc oxidized in an electrolyte containing EDTA-2Na (0.04 $M \cdot L^{-1}$) and NaOH (0.175 $M \cdot L^{-1}$) at 450 V for 5 min. Next, the microarc oxidized implants were hung in a PTFE cup but soaked with 40 mL bulk

solution (distilled water 30 mL and ethanol 10 mL) containing 0.7 g of NaOH and 0.5 g of $SnCl_4 \cdot 5H_2O$. Then, the steel vessel containing the PTFE cup were treated at 200 °C for 24 h. The surface modified implants were labelled according to the surface structure (Table S1).

Surface characterization. Surface morphology of the implants was observed by scanning electron microscopy (SEM, Helios Nanolab 600i, FEI Co., USA). The elemental composition of the surface with different features was investigated by an energy dispersive X-ray spectrometer (EDAX, USA) equipped with the SEM system. X-ray diffraction (XRD, D/max-gB, Japan) and Raman spectroscopy (Raman, Jobin Yvon, France) were used to analyze the phase composition of the smooth and rough implants, respectively. The phase and elemental composition of the nanorod formed on R-Ti-TiO_2-SnO_2 surface was further analyzed by transmission electron microscopy (TEM, Tecnai G2F30, FEI Co., USA) instrument via high resolution TEM and EDS. Reflectance spectra from 900-200 nm were recorded via UV-vis spectrophotometer (UV-2600, Shimadzu, Japan) to calculate the band gap for the semi-conductor layer on Ti-TiO_2, Ti-SnO_2 and Ti-TiO_2-SnO_2. The LSV curves of the samples were scanned from 0 V to 3 V versus SCE (saturated calomel reference electrode) by electrochemical workstation (CHI760E, Shanghai Chenhua Instrument, China), and 0.5 M Na_2SO_4 was used as the electrolyte.

***In vivo* Experiments.** All the animal experiments were approved by the animal care and experiment committee of Xi'an Jiaotong University College of Medicine complied with the approved guidelines. The detailed animal experimental methods have been reported in our previous works. [14,30,50] Twelve New Zealand rabbits (2.5–3 kg for each) were used in this work. During the surgery, three holes (Φ 2 × L6 mm^3) were drilled on each tibia of rabbit. And the Ti,

Ti-TiO_2 and Ti-TiO_2-SnO_2 implants were placed on the left leg, while the R-Ti, R-Ti-TiO_2 and R-Ti-TiO_2-SnO_2 were placed on the right leg (Figure S6).

After healing of 12 weeks, the rabbits were sacrificed to investigate the osseointegration of implants with different surface structures. X-ray 3D imaging system (Y. Cheetah, YXLON International GmbH, Germany) was used to rebuild the biological tissue around the implants in the region of interest (ROI) ($\Phi 3 \times L6$ mm^3) with an isotropic resolution of 8 μm. For morphometric measurement in ROI, the biological tissue volume (BV), total volume without the implant (TV) and biological tissue surface area (BS) were analyzed by VG Studio 2.1V. The Van Gieson (VG) stained transverse histological sections were observed by OLYMPUS microscope (CXX41, OLYMPUS, Japan) with a normal light source. The histomorphometrical measurement of the bone tissue with a distance of 500 μm to the cylindrical surface of implant was analyzed by ImageJ (Figure S7). The push-out force of the placed implants was measured by a universal testing machine (Instron-1186, Instron Co., USA).

Statistical Analysis. For the biomechanical test, six rabbits were used (n=6). Regard to each of the histological and micro-CT analysis, three rabbits were used (n=3). The student analysis of variance was used to calculate the statistical significance of difference by IBM SPSS statistical software package. The p values < 0.05 were considered statistically significant difference.

ASSOCIATED CONTENT

Supporting Information. The Supporting Information is available free of charge on the ACS Publications website. EDS analysis of R-Ti at the gouge area (Figure S1), SEM

morphology of the R-Ti-TiO_2-SnO_2 (Figure S2), weight of the modified Ti implants with different surface structure (Figure S3), Raman spectra of Ti-TiO_2 and Ti-TiO_2-SnO_2 (Figure S4), EDS analysis of the pushed-out Ti-TiO_2-SnO_2 in cortical bone region (Figure S5), X-ray radiographs of the tibia with placed implants (Figure S6), and schematic diagram for the histological morphometry of the VG stained sections (Figure S7); sample code based on the structure of implants (Table S1), and comparison of push-out test results of the Ti implant fabricated by different modified strategies (Table S2) have been used as supporting information in this work.

AUTHOR INFORMATION

Corresponding Author

* Yong Han. E-mail: yonghan@xjtu.edu.cn

* Bo Su. E-mail: b.su@bristol.ac.uk

Notes

The authors declare that there is no conflict of interest.

ACKNOWLEDGMENT

The authors gratefully acknowledge the financial support by the State Key Program of National Natural Science Foundation of China (Grant No. 51631007), National Natural Science Foundation of China (Grant No. 51602251), China Postdoctoral Science Foundation (Grant No.

2016M590941 and 2017T100745), and Fundamental Research Funds for the Central Universities (Grant No. xjj2017052). Rui Zhou also gratefully acknowledge the financial support for his research visit at the University of Bristol from the China Scholarship Council (Grant No. 201706285046).

REFERENCES

(1) Chen, Q. Z.; Thouas, G. A. Metallic Implant Biomaterials. *Mater. Sci. Eng., R* **2015**, *87*,1−57.

(2) Steflik, D. E.; Corpe, R. S.; Young, T. R.; Sisk, A. L.; Parr, G. R. The Biologic Tissue Responses to Uncoated and Coated Implanted Biomaterials. *Adv. Dent. Res*. **1999**, *13*, 27−33.

(3) Fujibayashi, S.; Neo, M.; Kim, H. M.; Kokubo, T.; Nakamura, T. Osteoinduction of Porous Bioactive Titanium Metal. *Biomaterials* **2004**, *25*, 443−450.

(4) Nasab, M. B.; Hassan, M. R.; Sahari, B. B. Metallic Biomaterials of Knee and Hip − A Review. *Trends Biomater. Artif. Organs* **2010**, *24*, 69−82.

(5) Mulari, M. T. K.; Qu, Q.; Harkonen, P. L.; Vaananen, H. K. Osteoblast-Like Cells Complete Osteoclastic Bone Resorption and Form New Mineralized Bone Matrix in vitro. *Calcif. Tissue Int.* **2004**, *75*, 253−261.

(6) Mori, S.; Burr, D. B. Increased Intracortical Remodeling Following Fatigue Damage. *Bone* **1993**, *14*, 103−109.

(7) Smit T. H.; Burger E. H. Is BMU-Coupling a Strain-Regulated Phenomenon? A Finite Element Analysis. *J. Bone Miner. Res.* **2000**, *15*, 301−307.

(8) Thiel A.; Reumann M. K.; Boskey A.; Wischmann J.; Eisenhart-Rothe R.; Mayer-Kuckuk P.

Osteoblast Migration in Vertebrate Bone. *Biol. Rev.* **2017**, *93*, 350−363.

(9) Wu, S. L.; Liu, X. M.; Yeung, K. W. K.; Liu, C. S.; Yang, X. J. Biomimetic Porous Scaffolds for Bone Tissue Engineering. *Mater. Sci. Eng., R* **2014**, *80*,1−36.

(10) Liu, X.; Wu, S.; Yeung, K. W.; Chan, Y. L.; Hu, T.; Xu, Z. S.; Liu, X. Y.; Chung, J. C. Y.; Cheung, K. M. C.; Chu, P. K. Relationship between Osseointegration and Superelastic Biomechanics in Porous NiTi Scaffolds. *Biomaterials* **2011**, *32*, 330–338.

(11) Zhou, R.; Wei, D. Q.; Feng, W.; Cheng, S.; Yang, H. Y.; Li, B. Q.; Wang, Y. M.; Jia, D. C.; Zhou, Y. Bioactive Coating with Hierarchical Double Porous Structure on Titanium Surface Formed by Two-Step Microarc Oxidation Treatment. *Surf. Coat. Technol.* **2014**, *252*, 148−156.

(12) Yan, Y. Y.; Sun, J. F.; Han, Y.; Li, D. C.; Cui, K. Microstructure and Bioactivity of Ca, P and Sr Doped TiO_2 Coating Formed on Porous Titanium by Micro-Arc Oxidation. *Surf. Coat. Technol.* **2010**, *205*, 1702−1713.

(13) Yerokhin, A. L.; Nie, X.; Leyland, A.; Matthews, A.; Dowey, S. J. Plasma Electrolysis for Surface Engineering. *Surf. Coat. Technol.* **1999**, *122*, 73−93.

(14) Bai, Y. X.; Zhou, R.; Cao, J. Y.; Wei, D. Q.; Du, Q.; Li, B. Q.; Wang, Y. M.; Jia, D. C.; Zhou Y. Microarc Oxidation Coating Covered Ti Implants with Micro-Scale Gouges Formed by A Multi-Step Treatment for Improving Osseointegration. *Mater. Sci. Eng., C* **2017**, *76*, 908–917.

(15) Girard, P. P.; Cavalcanti-Adam, E. A.; Kemkemer, R.; Spatz, J. P. Cellular Chemomechanics at Interfaces: Sensing, Integration and Response. *Soft Mater.* **2007**, *3*, 307–326.

(16) Ryan, G.; Pandit, A.; Apatsidis, D. P. Fabrication Methods of Porous Metals for Use in

Orthopaedic Applications. *Biomaterials* **2006**, *27*, 2651−2670.

(17) Sjostrom, T.; McNamara, L. E.; Meek, R. M. D.; Dalby, M. J.; Su, B. 2D and 3D Nanopatterning of Titanium for Enhancing Osteoinduction of Stem Cells at Implant Surfaces. *Adv. Healthcare Mater.* **2013**, *2*, 1285−1293.

(18) Zhou, J. H.; Li, B.; Lu, S. M.; Zhang, L.; Han, Y. Regulation of Osteoblast Proliferation and Differentiation by Interrod Spacing of Sr-HA Nanorods on Microporous Titania Coatings. *ACS Appl. Mater. Interfaces* **2013**, *5*, 5358–5365.

(19) Nepal, M.; Li, L.; Bae, T. S.; Kim, B.; Soh, Y. Evaluation of Osseointegration around Tibial Implants in Rats by Ibandronate-Treated Nanotubular Ti-32Nb-5Zr Alloy. *Biomol. Ther.* **2014**, *22*, 563–569.

(20) Yan, J.; Sun, J. F.; Chu, P. K.; Han, Y.; Zhang, Y. M. Bone Integration Capability of A Series of Strontium-Containing Hydroxyapatite Coatings Formed by Micro-Arc Oxidation. *J. Biomed. Mater. Res., Part A* **2013**, *101*, 2465–2480.

(21) Rajabi, A. H.; Jaffe, M.; Arinzeh, T. L. Piezoelectric Materials for Tissue Regeneration: A Review. *Acta Biomater.* **2015**, *24*, 12−23.

(22) Campetelli, A.; Bonazzi, D.; Minc, N. Electrochemical Regulation of Cell Polarity and the Cytoskeleton. *Cytoskeleton* **2012**, *69*, 601−612.

(23) Ning, C.; Zhou, L.; Tan, G. Fourth-Generation Biomedical Materials. *Mater. Today* **2015**, *19*, 2−3.

(24) Liao, J.; Zhu, Y.; Zhou, Z.; Chen, J.; Tan, G.; Ning, C.; Mao, C. Reversibly Controlling Preferential Protein Adsorption on Bone Implants by Using An Applied Weak Potential as A

Switch. *Angew. Chem. Int. Edit.* **2014**, *53*, 13068−13072.

(25) Ning, C.; Yu, P.; Zhu, Y.; Yao, M.; Zhu, X.; Wang, X.; Lin, Z.; Li, W.; Wang, S.; Tan, G.; Zhang, Y.; Wang, Y.; Mao, C. Built-in Microscale Electrostatic Fields Induced by Anatase-Rutile-Phase Transition in Selective Areas Promote Osteogenesis. *NPG Asia Mater.* **2016**, *8*, e243.

(26) Pfeifer, V.; Erhart, P.; Li, S.; Rachut, K.; Morasch, J.; Brötz, J.; Reckers, P.; Mayer, T.; Rühle, S.; Zaban, A.; Seró, I. M.; Bisquert, J.; Jaegermann, W.; Klein, A. Energy Band Alignment between Anatase and Rutile TiO_2. *J. Phys. Chem. Lett.* **2013**, *4*, 4182–4187.

(27) Scanlon, D. O.; Dunnill, C. W.; Buckeridge, J.; Shevlin, S. A.; Logsdail, A. J.; Woodley, S. M.; Catlow, C. R. A.; Powell, M. J.; Palgrave, R. G.; Parkin, I. P.; Watson, G. W.; Keal, T. W.; Sherwood, P.; Walsh, A.; Sokol, A. A. Band Alignment of Rutile and Anatase TiO_2. *Nat. Mater.* **2013**, *12*, 798–801.

(28) Mobini, S.; Talts, Ü. L.; Xue, R. K.; Cassidy, N. J.; Cartmell, S. H. Electrical Stimulation Changes Human Mesenchymal Stem Cells Orientation and Cytoskeleton Organization. *J. Biomater. Tissue Eng.* **2017**, *7*, 829–833.

(29) Marino, A. A.; Becker, R. O. Piezoelectric Effect and Growth Control in Bone. *Nature* **1970**, *228*, 473–474.

(30) Zhou, R.; Han, Y.; Cao, J. Y.; Li, M.; Jin, G. R.; Luo, H. T.; Zhang, L. Z.; Su, B. Electrically Bioactive Coating on Ti with Bi-layered SnO_2-TiO_2 Hetero-Structure for Improving Osseointegration. *J. Mater. Chem. B* **2018**, *6*, 3989−3998.

(31) Zhou, R.; Wei, D. Q.; Cao, J. Y.; Feng, W.; Cheng, S.; Du, Q.; Li, B. Q.; Wang, Y. M.; Jia, D.

C.; Zhou, Y. Conformal Coating Containing Ca, P, Si and Na with Double-Level Porous Surface Structure on Titanium Formed by A Three-Step Microarc Oxidation. *RSC Adv.* **2015**, *5*, 28908−28920.

(32) Liang, P.; Liao, C.; Chueh, C.; Zuo, F.; Williams, S. T.; Xin, X.; Lin, J.; Jen, A. K. Y. Additive Enhanced Crystallization of Solution-Processed Perovskite for Highly Efficient Planar-Heterojunction Solar Cells. *Adv. Mater.* **2014**, *26*, 3748–3754.

(33) Kudo, A.; Miseki, Y. Heterogeneous Photocatalyst Materials for Water Splitting. *Chem. Soc. Rev.* **2009**, *38*, 253–278.

(34) Li, J. H.; Wang, J. X.; Wang, D. H.; Guo, G. Y.; Yeung, K. W. K.; Zhang, X. L.; Liu, X. Y. Band Gap Engineering of Titania Film through Cobalt Regulation for Oxidative Damage of Bacterial Respiration and Viability. *ACS Appl. Mater. Interfaces* **2017**, *9*, 27475−27490.

(35) Kulbir, K.; Singh, C. V. Amorphous TiO_2 as A Photocatalyst for Hydrogen Production: A DFT Study of Structural and Electronic Properties. *Energy Procedia* **2012**, *29*, 291–299.

(36) Huang, J.; Liu, Y.; Lu, L.; Li, L. The Photocatalytic Properties of Amorphous TiO_2 Composite Films Deposited by Magnetron Sputtering. *Res. Chem. Intermed.* **2012**, *38*, 487–498.

(37) Sekiya, T.; Ohta, S.; Kamei, S. Hanakawa, M.; Kurita, S. Raman Spectroscopy and Phase Transition of Anatase TiO_2 under High Pressure. *J. Phys. Chem. Solids* **2001**, *62*, 717–721.

(38) Frank, O.; Zukalova, M.; Laskova, B.; Kurti, J.; Koltai, J.; Kavan, L. Raman Spectra of Titanium Dioxide (Anatase, Rutile) with Identified Oxygen Isotopes. *Phys. Chem. Chem. Phys.* **2012**, *14*, 14567–14572.

(39) Azam, A.; Habib, S. S.; Salah, N. A.; Ahmed, F. Microwave-Assisted Synthesis of SnO_2

Nanorods for Oxygen Gas Sensing at Room Temperature. *Int. J. Nanomed.* **2013**, *8*, 3875–3882.

(40) Tenkyong, T.; Mary, J. S. S.; Praveen, B.; Pugazhendhi, K.; Sharmila, D. J.; Shyla, J. M.; Structural Modulation and Band Gap Optimization of Electrochemically Anodized TiO_2 Nanotubes. *Mater. Sci. Semicond. Process.* **2018**, *83*, 150–158.

(41) Chen, J. H.; Liu, C.; You, L.; Simmons, C. A. Boning up on Wolff's Law: Mechanical Regulation of the Cells that Make and Maintain Bone. *J. Biomech.* **2010**, *43*, 108−118.

(42) Cox, B. N.; Smith, D. W. On Strain and Stress in Living Cells. *J. Mech. Phys. Solids* **2014**, *71*, 239−252.

(43) Kurata, K.; Uemura, T.; Nemoto, A.; Tateishi, T.; Murakami, T.; Higaki, H.; Miura, H.; Iwamoto, Y. Mechanical Strain Effect on Bone□Resorbing Activity and Messenger RNA Expressions of Marker Enzymes in Isolated Osteoclast Culture. *J. Bone Miner. Res.* **2001**, *16*, 722–730.

(44) Harada, S.; Rodan, G. A. Control of Osteoblast Function and Regulation of Bone Mass. *Nature* **2003**, *423*, 349–355.

(45) Martin, R. B. On the Histologic Measurement of Osteonal BMU Activation Frequency. *Bone* **1994**, *15*, 547–549.

(46) Jerez, S.; Camacho, A. Bone Metastasis Modeling Based on the Interactions between the BMU and Tumor cells. *J. Comput. Appl. Math.* **2018**, *330*, 866–876.

(47) Klein, N. J.; Veldhuijzen, J. P.; Strien, M. E.; de Jong, M.; Burger, E. H. Inhibition of Osteoclastic Bone Resorption by Mechanical Stimulation in vitro. *Arthritis Rheumatol.* **1990**, *33*, 66–72.

(48) Maejima-Ikeda, A.; Aoki, M.; Tsuritani, K.; Kamioka, K.; Hiura, K.; Miyoshi, T.; Hara, H.; Takano-Yamamoto, T.; Kumegawa, M. Chick Osteocyte-Derived Protein Inhibits Osteoclastic Bone Resorption. *Biochem. J.* **1997**, *322*, 245–250.

(49) Mackie, E. Osteoblasts: Novel Roles in Orchestration of Skeletal Architecture. *Int. J. Biochem. Cell Biol.* **2003**, *35*, 1301–1305.

(50) Zhou, R.; Wei, D. Q.; Cao, J. Y.; Feng, W.; Cheng, S.; Du, Q.; Li, B. Q.; Wang, Y. M.; Jia, D. C.; Zhou, Y. Synergistic Effects of Surface Chemistry and Topologic Structure from Modified Microarc Oxidation Coatings on Ti Implants for Improving Osseointegration. *ACS Appl. Mater. Interfaces* **2015**, *7*, 8932–8941.

(51) Gittens, R. A.; McLachlan, T.; Olivares-Navarrete, R.; Cai, Y.; Berner, S.; Tannenbaum, R.; Schwartz, Z.; Sandhage, K. H.; Boyan, B. D. The Effects of Combined Micron-/Submicron-Scale Surface Roughness and Nanoscale Features on Cell Proliferation and Differentiation. *Biomaterials* **2011**, *32*, 3395–3403.

(52) Horie, M.; Fujita, K. Chapter Four - Toxicity of Metal Oxides Nanoparticles. *Adv. Mol. Toxicol.* **2011**, *5*, 145–178.

(53) Ventre, M.; Causa, F.; Netti, P. A. Determinants of Cell-Material Crosstalk at the Interface: Towards Engineering of Cell Instructive Materials. *J. R. Soc. Interface* **2012**, *9*, 2017–2032.

(54) Xia, L.; Zhang, N.; Wang X.; Zhou, Y.; Mao, L.; Liu, J.; Jiang, X.; Zhang, Z.; Chang, J.; Lin, K.; Fang, B. The Synergetic Effect of Nano-Structures and Silicon-Substitution on the Properties of Hydroxyapatite Scaffolds for Bone Regeneration. *J. Mater. Chem. B* **2016**, *4*, 3313−3323.

(55) Fleig, A.; Penner, R. The TRPM Ion Channel Subfamily: Molecular, Biophysical and

Functional Features. *Trends Pharmacol. Sci.* **2004**, *25*, 633–639.

(56) Abed, E.; Moreau, R. Importance of Melastatin-Like Transient Receptor Potential 7 and Cations (Magnesium, Calcium) in Human Osteoblast-Like Cell Proliferation. *Cell Proliferation* **2007**, *40*, 849–865.

(57) Cheng, H.; Feng, J. M.; Figueiredo, M. L.; Zhang, H.; Nelson, P. L.; Marigo, V.; Beck, A. Transient Receptor Potential Melastatin Type 7 Channel Is Critical for the Survival of Bone Marrow Derived Mesenchymal Stem Cells. *Stem Cells Dev.* **2010**, *19*, 1393–1403.

(58) Abed, E.; Martineau, C.; Moreau, R. Role of Melastatin Transient Receptor Potential 7 Channels in the Osteoblastic Differentiation of Murine MC3T3 Cells. *Calcif. Tissue Int.* **2011**, *88*, 246–253.

(59) Couchourel, D.; Aubry, I.; Delalandre, A.; Lavigne, M.; Martel-Pelletier, J.; Pelletier, J. P.; Lajeunesse, D. Altered Mineralization of Human Osteoarthritic Osteoblasts Is Attributable to Abnormal Type I Collagen Production. *Arthritis Rheumatol.* **2009**, *60*, 1438–1450.

(60) Fan, X.; Feng, B.; Liu, Z.; Tan, J.; Zhi, W.; Lu, X.; Wang, J.; Weng, J. Fabrication of TiO_2 Nanotubes on Porous Titanium Scaffold and Biocompatibility Evaluation in vitro and in vivo. *J. Biomed. Mater. Res., Part A* **2012**, *100A*, 3422–3427.

(61) Peng, Wei.; Xu, L.; You, J.; Fang, L.; Zhang, Q. Selective Laser Melting of Titanium Alloy Enables Osseointegration of Porous Multi□Rooted Implants in A Rabbit Model. *BioMed. Eng. OnLine.* **2016**, *15*, 85.

(62) Wang, Q.; Qiao, Y.; Cheng, M.; Jiang, G.; He, G.; Chen, Y.; Zhang, X.; Liu, X. Tantalum Implanted Entangled Porous Titanium Promotes Surface Osseointegration and Bone Ingrowth.

Sci. Rep. **2016**, *6*, 26248.

(63) Zhou, R.; Wei, D. Q.; Cheng, S.; Feng, W.; Du, Q.; Yang, H. Y.; Li, B. Q.; Wang, Y. M.; Jia, D. C.; Zhou, Y. Structure, MC3T3-E1 Cell Response, and Osseointegration of Macroporous Titanium Implants Covered by A Bioactive Microarc Oxidation Coating with Microporous Structure. *ACS Appl. Mater. Interfaces* **2014**, *6*, 4797–4811.

Table of Contents